A flavin-based extracellular electron transfer strategy in a novel gram-positive microbe *Microbacterium deferre* sp. nov. strain A1-JK, isolated from cable bacteria enrichments

Jamie J.M. Lustermans[1,2]*, Naja Basu[3], Kartik Aiyer[4]*

[1]Microbial Systems Technology Excellence Centre, University of Antwerp, Belgium

[2]Department of Biology, Research Group Geobiology, University of Antwerp, Wilrijk, Belgium

[3] Department of Biology, Aarhus University, Aarhus, Denmark 8000

[4] Department of Biology, Center for Electromicrobiology, Aarhus University, Aarhus, Denmark 8000

*Corresponding authors: kartikaiyer@bio.au.dk; Jamie.lustermans@uantwerpen.be

Abstract

Microbacteriaceae are a class of metabolically versatile gram-positive bacteria found in diverse environments. In sediments populated with filamentous cable bacteria, electric interspecies interactions between microbes and cable bacteria have been suggested. A novel, gram-positive bacterium, *Microbacterium deferre* strain A1-JK was isolated from the vicinity of a cable bacterium filament, capable of extracellular electron transfer (EET) to Fe(III) oxides and electrodes. Electrochemical experiments with pure cultures of *M.deferre* A1-JK in three-electrode cells revealed the presence of soluble mediators diffusing through the cell wall, identified through HPLC analysis as flavins. Genomic analyses further uncovered the complete riboflavin synthesis pathway, with heightened flavin production observed under oxygen-limited conditions to facilitate EET. *M. deferre* A1-JK encodes the periplasmic cytochrome FccA, responsible for transferring electrons on flavin carriers. *M. deferre* A1-JK exhibited a fast switch from aerobic metabolism to EET-based metabolism, aside from demonstrating weak electroactivity in alkaline (pH 8-10) and saline (4% NaCl) conditions. These results underscore its adaptability to use EET as an efficient survival strategy to deal with rapidly fluctuating sediment environments. These results hold promise for elucidating metabolic dynamics at oxic-anoxic interfaces along with further understanding of biogeochemical cycling in sediments.

Keywords: Microbacterium, extracellular electron transfer, electrode, flavins, gram-positive

Introduction

Extracellular electron transfer (EET) is a process in which microbes exchange electrons with extracellular acceptors and donors for energy generation. A defining feature of electroactive microbes, EET is often employed as a strategy to gain access to distant and scarce electron acceptors in the absence of soluble alternatives. Electroactive microbes can use different mechanisms to mediate EET. Direct electron transfer relies on conductive nanowires and outer membrane cytochromes to perform EET via surface contact[1,2]. Mediated electron transfer, on the other hand, uses soluble redox shuttles that diffuse inside and outside the cell to ultimately reduce an external electron acceptor[3–5].

In recent years, electroactivity has expanded beyond the model organisms *Shewanella oneidensis* and *Geobacter sulfurreducens*[6]. Several other microbes, which were originally not viewed through the lens of electroactivity have since been discovered to be electroactive. These include the gram-positive microbes *Enterococcus faecalis*[7,8], *Listeria monocytogenes*[9], *Lactiplantibacillus plantarum*[10] and *Paraclostridium* species[11]. Electroactive microbes have been discovered in several different ecosystems, as electroactivity plays a key role in adapting to nutrient/oxygen limited zones in changing environments[12]. Sulfidic freshwater and marine sediments populated by cable bacteria are examples of such environments. Cable bacteria are filamentous, sulfide-oxidizing bacteria present ubiquitously in freshwater and marine sediments[13–15]. Cable bacteria spatially segregate redox half-reactions and link them via long-distance electron transport through periplasmic wires over centimetre distances[15]. Distinct biogeochemical gradients of oxygen, sulfide and pH are created in sediments due to the electrochemical activity of cable bacteria[16]. In such sediments, a "microaerophilic" veil with trace amounts of oxygen is commonly observed, inhabited by (micro)aerobic bacteria, which are often facultative [17,18].

It was discovered that other microbes "flock" around cable bacteria to indirectly access oxygen via the cable bacteria filaments[19]. This intriguing phenomenon was proposed to happen through interspecies EET and raises possibilities of studying not only interspecies interactions, but also the role of electroactivity in flocking microbes in such a dynamic environment[19,20]. A novel species *Microbacterium deferre* strain A1-JK was isolated from the microaerophilic veil of an enrichment of freshwater cable bacteria[29] and studied here as a potential flocking candidate.

The genus *Microbacterium* is gram-positive and is found in diverse environmental conditions. These include a high-altitude desert environment[21], human clinical specimens[22] and a radioactive waste site[23]. As a polyextremophile it can grow under several different conditions: this freshwater species is a psychrophile[24], a halophile[25], grows under a wide range of pH conditions (5-11)[26] and is facultatively aerobic. In pure cultures, *M. deferre* A1-JK produces yellowish pigmented colonies and can utilise several carbon sources, as most others of this genus[27]. Our experiments demonstrate that it can respire anaerobically through EET mediated by flavins. We present the mechanism of EET in *M. deferre* A1-JK along with a potential model for its electron transfer, supported by physiological and genomic analyses. Further, it exhibits a rapid switch from aerobic metabolism to EET-based metabolism, probably in response to fluctuating conditions in sediments. The implications of EET in *M. deferre* A1-JK, its interspecies interactions and potential applications are also discussed.

Materials and Methods

Isolation

A trench slide was used to inoculate sediment containing freshwater cable bacterium *Electronema aureum* GS[28] as per Bjerg et al[15]. Microaerophilic veils are characteristically formed in trench slides as oxygen diffuses into the trench slide. After cable bacteria were observed stretching out from the trench, visualized capillary suction was employed to draw out the liquid from the microaerophilic veil, as described earlier by Lustermans et al [29]. Following plating on Reasoners 2-A agar plates, *M. deferre* A1-JK colonies were identified and

transferred under laminar air flow to sterile agar plates to obtain pure cultures. The agar plates were incubated aerobically in dark conditions at 15 °C.

Physiological testing

API 20E and 20NE test strips (Biomérieux) were inoculated and read according to the manual. Strips were incubated in the dark at room temperature for 24 hours initially, and subsequently for 48 and 72 hours. Growth was determined at different temperatures: 4°C, 15°C, 18-22°C (room temperature), and 37.5°C, by inoculating and incubating Nutrient Broth (NB), VWR, R2A (Millipore) and Luria-Bertani (VWR) agar plates in the dark. Similarly, growth in incremental salt concentrations 1-4%, and 10% NaCl in LB plates were tested. Since LB contains 1% NaCl, R2A plates were used for 0% NaCl.

Nutrient medium composition for electrochemical cells

A defined nutrient medium was prepared for electrochemical studies. The nutrient medium was modified *Shewanella* basal medium, consisting of the following components (per litre): K_2HPO_4, 0.225 g; KH_2PO_4, 0.225 g; NaCl, 0.46 g; $(NH_4)_2SO_4$, 0.225 g; $MgSO_4 \cdot 7\ H_2O$, 0.117 g; HEPES, 23.83 g. Sodium succinate (20 mM) was used as carbon source. Mineral and vitamin mix (5 ml each) was added. The mineral mix consisted of nitrilotriacetic acid, 1.5 g; $MnCl \cdot 4\ H_2O$, 0.1 g; $FeSO_4 \cdot 7\ H_2O$, 0.3 g; $CoCl_2 \cdot 6\ H_2O$, 0.17 g; $ZnCl_2$, 0.1g; $CuSO_4 \cdot 5\ H_2O$, 0.04 g; $AlK(SO_4)_2 \cdot 12\ H_2O$, 0.005 g; H_3BO_3, 0.005 g; Na_2MoO_4, 0.09 g; $NiCl_2$, 0.12 g; $NaW_4 \cdot 2\ H_2O$, 0.02 g and Na_2SeO_4, 0.1 g (per litre), while the vitamin mix consisted of folic acid, 0.002 g; biotin, 0.002 g; pyridoxine HCl, 0.02 g; thiamine, 0.005 g; nicotinic acid, 0.005 g; pantothenic acid, 0.005 g; cyanocobalamin, 0.0001 g; p-aminobenzoic acid, 0.005 g and thioctic acid, 0.005 g.

Electrochemical cell construction

Three-electrode cells fabricated from glass bottles (30ml working volume) were used as electrochemical reactors. The working electrode consisted of carbon felt (Thermo Fisher, dimensions 2 cm × 2 cm × 0.3 cm), Ag/AgCl (REF201 Radiometer Analytical, Denmark) constituted the reference electrode and a Pt wire was used as the counter electrode. The cells were inoculated with 3 ml (10% inoculum) of *Microbacterium* culture (OD 0.4), followed by addition of 27ml nutrient medium. After inoculation, nitrogen was sparged for 20 minutes to make the reactors anoxic, following which electrochemical experiments were conducted.

Electrochemical measurements

A potential of 200 mV was applied using a MultiSens4 (PalmSens) potentiostat for chronoamperometry (CA). Additionally, chronoamperometric measurements were performed under alkaliphilic and halophilic conditions (pH 8-10; 4% salt). Cyclic voltammetry (CV) was performed at a potential window from -0.6 V to +0.6 V at a scan rate of 1 mV. For Randles-Sevcik plots, CV was done at varying scan rates of 1 mV, 5 mV, 10 mV and 25 mV. Differential pulse voltammetry (DPV) was performed with the same scan window as cyclic voltammetry, using 1 s period, 0.3 s pulse time, 50 mV pulse size and 1 mV step size. EIS was done in potentiostatic mode based on midpoint potential of the cyclic voltammogram (-0.384 V). The potential amplitude was 30 mV.

At the end of the experiments, spent medium was analysed via CV and DPV. The electrolyte from the three-electrode cells was collected and centrifuged at 6000 g for 15 min, followed by collecting the supernatant and repeating the centrifugation for 30 min. The resulting

114 supernatant was filtered using a 0.22 µm membrane to obtain cell-free spent medium. The
115 spent medium was transferred to new three-electrode cells with fresh electrodes for
116 electrochemical studies.

117 CA, CV, DPV, Randles-Sevcik plots and EIS were all conducted in triplicates.

118 *Electrode switching experiments*

119 After operating the three-electrode cells for a period of 7 days, the electrodes and electrolyte
120 were separated in fresh reactors to ascertain redox-active components to elucidate the EET
121 mechanism. The electrodes were carefully transferred to new reactors with fresh nutrient
122 medium, while pristine electrodes were introduced into the old electrolyte.

123 *HPLC*

124 HPLC was done to quantify redox shuttles. Based on the redox peaks in cyclic
125 voltammograms, flavins were targeted for quantification by HPLC. Filtered spent medium from
126 three-electrode cells was used. HPLC was done on a Dionex UltiMate 3000 UPLC system
127 (Thermo Scientific) equipped with a C18 analytical column. Fluorescence of riboflavin was
128 monitored (excitation 440 nm; emission 525 nm). Final riboflavin concentration was
129 determined by eluting a series of riboflavin standards (100 nM, 200 nM, 400 nM, 800 nM, 1
130 µM, 2 µM and 3µM) and preparing a standard curve. Samples were run in triplicates.

131 *Gram staining*

132 Cells of *M. deferre* A1-JK were deposited onto a drop of milliQ water, airdried and heat-fixated
133 on a microscopy slide by moving through a flame. The sample was stained with crystal violet
134 for 1 min and thoroughly rinsed with milliQ water, followed by iodine solution flooding for 1 min
135 and rinsing. Decolouring was done for 2 s with 100% ethanol and rinsing. Safranine solution
136 was used for counterstaining for 30 s and rinsing. The slide was airdried and inspected with a
137 light microscope as described below.

138 *Microtiter Dish Biofilm Formation Assay*

139 The ability of *M. deferre* A1-JK to form biofilms was estimated by the microtiter dish biofilm
140 formation assay, as described previously[30,31]. Briefly, the cells from the three-electrode
141 reactors were diluted 1:100. 100µl of this culture was added in 96-well plates, followed by
142 addition of 125 µl of 0.1% crystal violet solution. Following incubation at room temperature for
143 15 minutes, the plates were washed with distilled water. After drying, 125µl of 30% acetic acid
144 was added in the wells. Absorbance was measured at 550nm.

145 *Light and Scanning Electron Microscopy (SEM)*

146 Plate culture of *M. deferre* A1-JK was put on glass microscopy slides, anoxic tap water was
147 added and covered with a glass coverslip. Light microscopy images were made with phase-
148 contrast at 1000x with an oil lens (Zeiss Axioplan 2), black and white camera (Exi Blue). SEM
149 samples were prepared by putting a carbon sticker on an aluminium SEM pin in a dust free
150 environment. Plate cultures, liquid cultures and carbon felt electrodes (after concluding the
151 electrochemical cell measurements) were deposited on the carbon sticker and dried for 24 h,
152 followed by vacuum gold-sputtering for 40s (Agar Sputter Coater). Images were made with a
153 Phenom ProX SEM (Phenom-World BV) using a backscattered electron detector with a 10 kV
154 electron beam.

155 Images were used to determine motility, spore formation, and measure cell size. Sizes were
156 measured using the measure tool in Fiji's ImageJ[32].

157 *DNA extraction, 16S gene- and genome sequencing*

158 As stated in Lustermans *et al*[29], 16S rRNA-based taxonomy was determined through a colony
159 PCR on a single colony of *M. deferre* A1-JK which was Sanger sequenced (Macrogen). A
160 second sample of multiple colonies of *M. deferre* A1-JK (also from an agar plate) was used
161 for DNA extraction with the DNeasy PowerSoil kit (Qiagen). Concentration and length quality
162 checks were done using Qubit (Fischer Scientific) and an Implen Spectrophotometer (Fischer
163 Scientific) according to the manual. Genomic DNA was sent for Illumina MiSeq sequencing
164 2x150bp (Eurofins, Germany).

165 *Genome assembly, annotation, analyses and phylogeny*

166 Trimming, size filtering and adapter removal was done with Trimmomatic v0.39 crop 125 and
167 headcrop 20 [33]. Trimmed paired-end reads were *de novo* assembled with SPAdes v3.15.5 with
168 parameters[34] isolate, default coverage cut-off and default k-mer values. Statistics for
169 completeness, contamination, quality, G+C content and coverage were calculated with Quast
170 v5.2.0[35], fastq-stats v1.01 and CheckM2 v1.0.1[36,37].

171 All available *Microbacterium* genomes were downloaded from NCBI genbank and used as
172 database for gene identification with PROKKA v1.14.5[38]. Before use, the database was
173 deduplicated with CD-HIT v4.8.1 with a length cut-off of 0.8, clustered into the most similar
174 cluster, and 0.9 sequence identity threshold[39,40].

175 Metabolic pathways were determined with BlastKOALA and KEGG mapper[41,42]. EET- and
176 electron shuttle synthesis genes were identified through blastp[43], using a manually, in-house
177 curated, protein database of EET-related genes with an E-value cut-off of 1E-6[29].

178 Phylogeny and taxonomic trees were determined with GTDB-Tk 2 infer and align[44], FastANI[45],
179 and Figtree2 (http://tree.bio.ed.ac.uk/software/figtree/) on all *Microbacterium* genomes from
180 NCBI, or a subset of the phylogenetic tree: a branch which contained A1. As outgroup,
181 *Mesorhizobium loti* LMG 6125 was used. ANI (http://enve-omics.ce.gatech.edu/ani/index) was
182 used to determine differences with the two closest relatives *M. hatanonis* JCM 14558 and *M.*
183 *sp.* Gd 4-13.

184 The genome of *M. deferre* A1-JK is accessible at NCBI genbank under the reference
185 PRJNA1125322.

186 **Results and Discussion**

187 *Current generation by A1-JK in electrochemical reactors*

188 The ability of *M.deferre* A1-JK to use the electrode as the electron acceptor was evaluated
189 electrochemically. After a lag phase of around 20 hours, current in the three-electrode cells
190 steadily increased with cell growth (Figure 1). All three-electrode reactors demonstrated a
191 similar trend: lag phase as the cells acclimatized to use the electrode as the electron acceptor,
192 rising current phase leading to a peak and finally a decrease in current. Current levels
193 increased steadily from ~10 μA at 24 hours and peaked at ~27 μA after 60 hours. The
194 subsequent decrease in current likely corresponded to a depletion of nutrients, as fresh
195 nutrient medium injection into the reactors increased the current to previous levels.

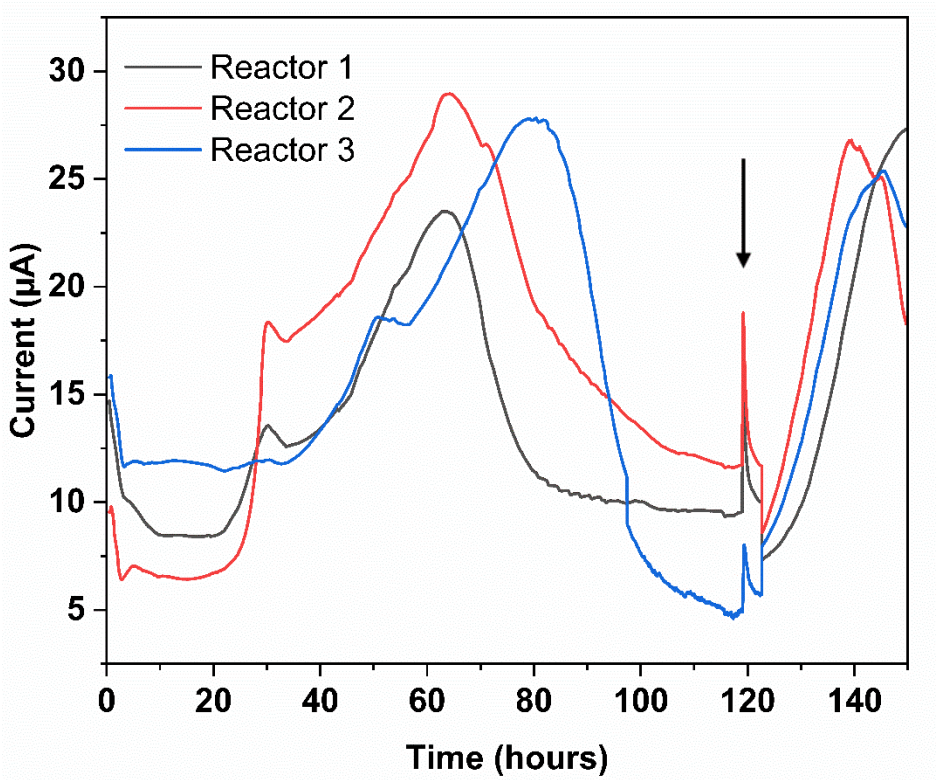

Figure 1: Chronoamperometric plots of *M.deferre* A1-JK from the three-electrode cells show a lag phase, log phase with increasing current and a decline in current. The arrow represents the time point at which fresh nutrient solution was injected.

Cell morphology and sizes of *M. deferre* A1-JK cultures on both the carbon felt and agar plates were compared through SEM (figure 2). On carbon felt electrodes, cells were seen as elongated ovoid-rods, and cell size recorded was 1.799 ± 0.35 × 0.672 ± 0.06 µM (figure 2a, 2b). More cells aggregated on the electrode over time, though a thick biofilm was not observed. The plate-grown cells, on the other hand, revealed short ovoids or spherical rods (1.097 ± 0.11 × 0.404 ± 0.06) that lumped together in a tight biofilm in yellow colonies (figure 2c). Such dimorphism has previously been observed for *Microbacterium* species to occur when cultures become older[27]. The sizes, and particularly the length of the electrode grown cells of A1-JK suggest that the cells were kept healthier for a much longer period than on an agar plate.

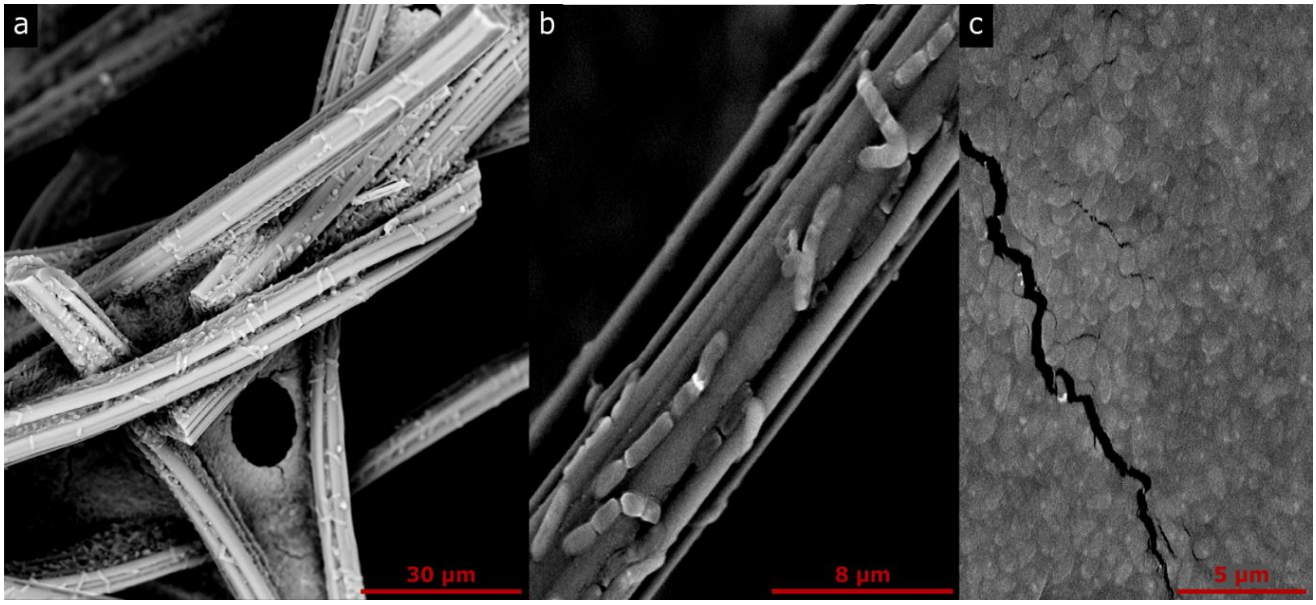

Figure 2: Scanning electron microscopy images of *M.deferre* A1-JK depicting elongated ovoid-rod cells on carbon felt electrodes (a, b) and short ovoid-rod cells on the agar plate (c).

Mode of electron transfer

Cyclic voltammetry produced a distinct redox couple at -0.302 V (figure 3a), suggesting the involvement of soluble redox shuttles mediating electron transfer. The CV shows a second oxidation peak, occurring at +0.18 V (figure 3a). This peak was, however, inconsistent in DPV (figure 3b), suggesting a smaller role in EET. Based on the potential, this peak was identified as soluble iron from the nutrient medium as demonstrated previously[46].

The peak heights at negative potentials increased in the CV and DPV over time, indicating a rise in redox shuttle concentrations (figure 3b). This suggested that there was a synthesis of potential redox shuttles, with concentrations correlated to cell growth. Randles–Ševčík plots (figure 3c) based on differing scan rates produced linear curves, confirming that electron transfer occurred by diffusion and that mediator concentration was the limiting factor in current generation.

EIS analysis corroborated the findings on diffusion-based electron transfer (figure 3d). As the cells in the reactor acclimatized to reduce the electrode, the resistance to charge transfer decreased, with the smallest resistance corresponding to the highest current generation. Interestingly, the development of biomass over the anode over time did not reduce charge transfer. This suggests that there may not have been a strong biofilm formation, and that the cells depended on mediators to perform electron transfer. Biofilm assays revealed weak ability of *M. deferre* A1-JK cells to form biofilms (figure S1).

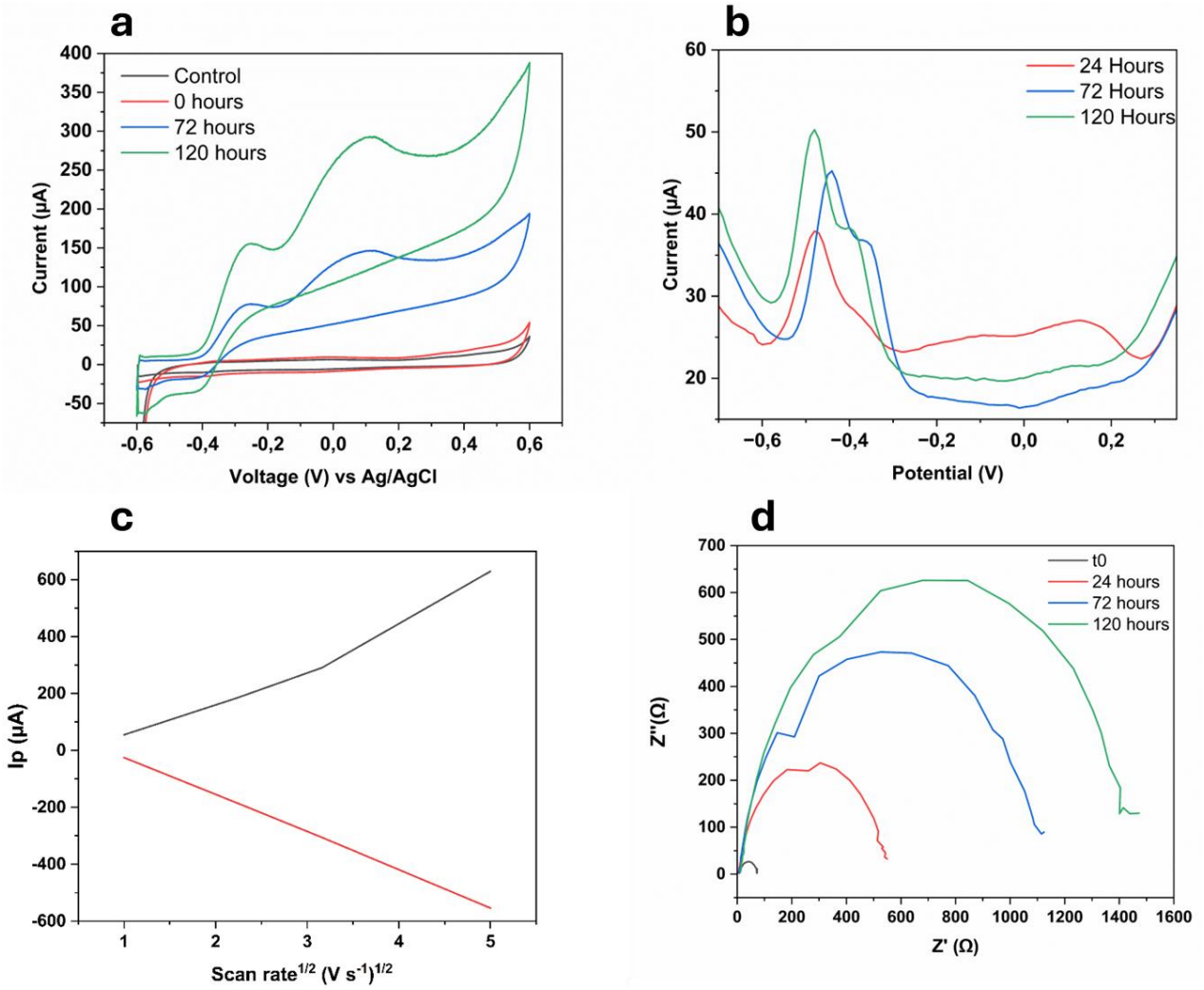

Figure 3a. Cyclic voltammograms of *M. deferre* A1-JK from electrochemical cells revealed redox couples at -0.302V. 3b. Differential pulse voltammetry produced peaks that increased over time, suggesting the involvement of redox shuttles. 3c. Randles–Ševčík plot of *M. deferre A1-JK* cultures confirmed that electron transfer occurred via diffusion. 3d. EIS plots for *M. deferre* A1-JK .

Electrode switching experiments and HPLC confirm flavin-mediated EET

By separating the electrolyte (spent medium without the cells) and the carbon-felt electrodes from the three-electrode cells we determined the degree of direct and mediated electron transfer by *M. deferre* A1-JK. DPV on reactors with fresh medium and used electrodes showed no redox peaks, implying an absence of components necessary for performing direct electron transfer (figure 4a). Redox peaks were clearly present with the previously used media, confirming the presence of secreted mediators.

HPLC analyses of the cell-free electrolyte confirmed the mediators to be riboflavin and flavin adenosine dinucleotide (FAD). This is consistent with reports of flavins occurring at similar negative potential in other studies[4,47,48]. Riboflavin was quantified, and concentrations increased from 200 nM after 24 hours to 1.6 µM after 6 days at peak current generation (figure S2). A test run of S.oneidensis MR-1 in the same electrochemical setup yielded riboflavin at a

concentration of 2.2 μM. Further, in reactors containing fresh electrodes in old electrolytes, riboflavin concentration was estimated at 1.4 μM. In reactors with fresh nutrient medium and previously used electrodes, riboflavin concentration after three days was only 100 nM, indicating that redox shuttles were secreted in the medium and direct electron transfer was minimal. When riboflavin was spiked into reactors containing previously used electrodes in fresh media, current generation increased from 5 μA to 35 μA (figure 4b), thereby confirming mediated electron transfer as the mode of EET.

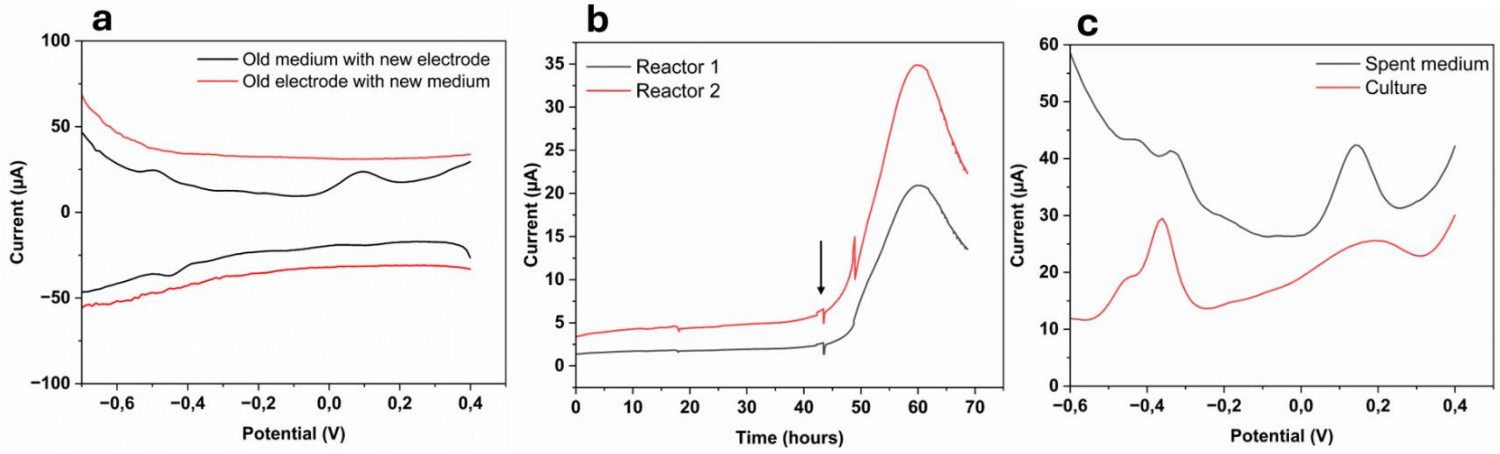

Figure 4a: DPV of electrode (red) and nutrient medium (black) revealed redox-active peaks in the medium. Mean values from triplicates are presented. 4b. Current instantly increased during chronoamperometry with external addition of riboflavin (arrow) in reactors with old electrodes in fresh nutrient medium. 4c. DPV of spent medium and culture from the three-electrode cell reveal peaks at similar potentials. Mean values from triplicates are reported.

Further, following the end of the experiment, the electrolyte was carefully collected and centrifuged. The supernatant was filtered, and the resulting spent media was analysed via DPV (figure 4c). Similar peaks were seen in the culture as well as the spent medium, validating the above results.

Versatility to perform EET in different conditions

M. deferre A1-JK demonstrated an ability to transition from aerobic respiration to EET-based metabolism. In three-electrode setups with stable current generation, oxygen was introduced by bubbling air for 20 minutes to observe its impact on EET (figure S3). Notably, the current declined from 16 μA at steady state to 4 μA upon oxygen saturation. However, within 35 minutes, there was a remarkable recovery as the current increased to ~90% of its previous levels, emphasizing that EET may be a commonly deployed mechanism in fluctuating sediment environments where *M. deferre* A1-JK is naturally present. Additionally, *M. deferre* A1-JK was tested in high pH (9, 10) conditions that can be encountered in the oxic zone in sediments[53]. Chronoamperometric plots at pH 9 and 10 showed a biological current signal, indicating electroactivity (figure S4). To determine whether *M. deferre* A1-JK was able to grow at different pH range (5-10), growth curves under aerobic and anaerobic conditions were done (figure S5). These showed that *M. deferre* A1-JK was adaptable to pH as long as oxygen was present, as no discernible growth occurred in anaerobic conditions.

M. deferre A1-JK also demonstrated weak electroactivity under 4% salt conditions (figure S4). Specific reasons behind the functionality of performing EET under high salt concentrations, however, remain unknown. Interestingly, *M. deferre* A1-JK was able to grow at salt concentrations ranging from 0-4% NaCl but grew very poorly at 10% NaCl and only after >10 days (table S1). The closest phylogenetic relative to M. *deferre* A1-JK, *Microbacterium sp*. Gd 4-13 demonstrated the ability to grow at salt concentrations of 10% NaCl (figure S6, S7)[25].

Potential EET routes

Potential EET pathways of *M. deferre* A1-JK based on genomic data is highlighted in figure 5. A partial route using the periplasmic proteins DmkA, DmkB, and Ndh2 might control electron fluxes towards aerobic respiration and EET [49]. This is similar to observations from other gram-positive electroactive microbes like *L. monocytogenes*. The periplasmic cytochrome FccA would be used to direct the electron flow from the quinone pool towards reduction of both riboflavin and FAD via FmnA. In previous studies where FccA and FmnA were genetically knocked out in *S.oneidensis*, ferric iron and fumarate reduction were suppressed, showing a clear involvement of FccA in EET[50].

Flavins are synthesized in *M.deferre* A1-JK, (with RibBA, RibD, RibE1,2), reduced with FmnA and then likely externalized via cell wall diffusion, as experimentally observed in the Randles–Ševčík plots (figure 3c). Curiously, both known flavin exporters Bfe and YeeO, were encoded in the genome, but neither has been reported to be capable of electron transport over cell walls[51]. However, recordings of such transporters in gram-positives are becoming more common, and knock-out studies might further elucidate their specific role in EET pathways[20,52].

After externalization, the flavins proceed to reduce extracellular electron acceptors. In sediments, the use of flavins as shuttles might lead to interspecies interactions with cable bacteria, as hypothesised earlier[19,53]. Outside of flavins, a synthesis pathway for phenazines was detected. Potentially, both flavins and phenazines could be used as mediators in EET. Yet only flavin signature peaks were detected in voltammetry measurements. The complex production and energetically expensive costs of phenazines likely prevented their synthesis in the low-energy nutrient medium that was used for the electrochemical cells. Another reason for the lack of phenazines could be that some of the genes from the phenazine synthesis operon were used in alternative biosynthetic pathways[54].

Interestingly, the outer membrane cytochrome ExtH, discovered in *G. sulfurreducens*, was encountered twice in the genome of *M. deferre* A1-JK. ExtH is involved in Se metal uptake in *G. sulfurreducens*[55,56]. The finding of a gram-negative outer membrane protein that forms an EET-related protein complex in a gram-positive bacterium is remarkable. However, both its cellular localization and its specific role in EET for *M. deferre* A1-JK are yet unclear. We propose that there may be a second periplasmatic protein to support faster internal electron transport but have not found any clear evidence. Further studies are required in this direction to elucidate the role of ExtH and any associated proteins.

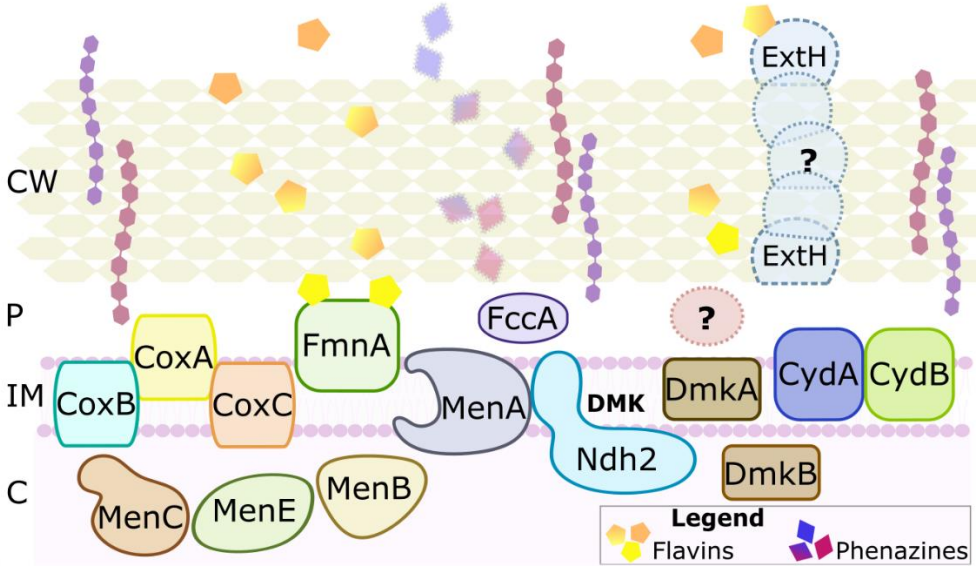

Figure 5: Potential extracellular electron transfer pathways in the genome of *Microbacterium deferre* A1-JK. CW: cell wall, P: periplasm, IM: inner membrane, C: cytoplasm, hexagonal strings represent teichoic acids.

Metabolic potential of M. deferre *A1-JK*

As stated above, *M. deferre* A1-JK has several potential pathways to interact with extracellular electron acceptors. With the large metabolic versatility documented in the *Microbacterium* genus[24-27], we investigated the genomic potential of *M. deferre* A1-JK towards drug degradation. Genomic analyses revealed the ability to degrade several different types of drugs, including polystyrene, $DMSO_2$ (dimethylsulfone or methylsulfonylmethane; MSM) and formaldehyde (figure S8). Further, the capability of breaking down (poly)sugars which it likely uses for assimilation, was also present, though growth on L-oriented amino acids is likely not possible. Assimilation of single or dual-chain sugars occurs only after 48-72 h, while fermentation of such sugars could occur after 24 h. *M. deferre* A1-JK was not capable of producing H_2S but may produce very small amounts of N_2 (table S1).

Conclusions

M. deferre A1-JK is the first reported gram-positive electroactive bacterium in class *Microbacteriaceae*. *M. deferre* A1-JK has a versatile metabolism where it can use many different carbon sources, including (poly)sugars. A flavin-mediated EET strategy is employed by *M. deferre* A1-JK under anaerobic conditions. Remarkably, the ability to mediate EET is present even in harsh conditions (pH 9-10 and 4% salt).

In sediments where cable bacteria are found, unique selection pressures like pH and oxygen fluctuations arise because of cable bacterial activity. Such an environment could create the necessary conditions for *M. deferre* A1-JK to rapidly transition to EET by using the minerals available as electron acceptors. The rapid switching of *M. deferre* A1-JK from aerobic metabolism to EET-based metabolism warrants further studies on metabolic adaptations in response to changing environmental conditions. Such studies will also be useful in further understanding its influence on the biogeochemistry and its role in nutrient cycling. It is worth examining the cell wall and associated proteins for any unique structural adaptations to combat high alkalinity and salt concentrations.

367 *M. deferre* A1-JK possesses the genomic potential to degrade formaldehyde, styrene and
368 dimethylsulfone, which may well be beneficial for designing applications. Examples could
369 include its use as a biosensor in detecting drug-waste in water supplies through current
370 generation, or extreme environment biosensors.

371 *Description of M. deferre A1-JK* sp. nov.

372 *Microbacterium deferre* (Lat. from *deferre/defero*; reduce, transport or exchange, after its
373 capabilities to transport and exchange electrons through the reduction of electron shuttles).
374 Cells are gram-positive, irregular and non-motile rods that become ovoid shaped when older
375 (1.1-1.8 µm × 0.4-0.7 µm). They form mucoid, faded-yellow colonies (3-6 mm diameter) but
376 colony color and size differ between growth media. *M. deferre* A1-JK is catalase positive, and
377 OF-test positive for glucose, arabinose and sucrose and weakly so for mannose, maltose and
378 gluconate. It is capable of growing on a wide range of complex growth media and may produce
379 low concentrations of N_2. NaCl concentrations of 10.0% (w/v) are poorly tolerated, with normal
380 growth occuring until at least 4.0%. Growth occurs aerobically or anaerobically at a pH range
381 from 5.0-10.0, and at a temperature range from 4°C to 37.5°C. The size of the genomic DNA
382 is ~3.5 Mb, with a G+C content of 69.32%.

383 *M. deferre* A1-JK was isolated from a microaerophilic veil that formed in a trench slide
384 containing freshwater sediment with a single strain of cable bacteria: *Electronema aureum*
385 GS[28,57]. The sample was extracted with a glass capillary in March 2019 and cultivated until a
386 pure culture was reached in June 2019. The accession number for *M. deferre* A1-JK genome
387 sequence is PRJNA1125322.

388

389 **Acknowledgments**

390 KA and JJML both acknowledge funding from the European Union's Horizon Research and
391 Innovation Program under the Marie Sklodowska-Curie grant agreement (project 101109777;
392 KA and 101152850; JJML). The authors thank Dimitri Stamatis for his assistance with the
393 HPLC and Jeanine S Geelhoed for logistical sequencing support. The Danish National
394 Research Foundation (Center for Electromicrobiology, DNRF136) is also acknowledged.

395

396 **References**

397 1. Busalmen, J.P., Esteve-Núñez, A., Berná, A., and Feliu, J.M. (2008). C-Type Cytochromes Wire
398 Electricity-Producing Bacteria to Electrodes. Angewandte Chemie *120*, 4952–4955.
399 https://doi.org/10.1002/ange.200801310.

400 2. Reguera, G., McCarthy, K.D., Mehta, T., Nicoll, J.S., Tuominen, M.T., and Lovley, D.R. (2005).
401 Extracellular electron transfer via microbial nanowires. Nature *435*, 1098–1101.
402 https://doi.org/10.1038/nature03661.

403 3. Glasser, N.R., Saunders, S.H., and Newman, D.K. (2017). The Colorful World of Extracellular
404 Electron Shuttles. Annu Rev Microbiol *71*, 731–751. https://doi.org/10.1146/annurev-micro-
405 090816-093913.

406 4. Marsili, E., Baron, D.B., Shikhare, I.D., Coursolle, D., Gralnick, J.A., and Bond, D.R. (2008).
407 Shewanella secretes flavins that mediate extracellular electron transfer (PNAS).

5. Aiyer, K.S. (2020). How does electron transfer occur in microbial fuel cells? World J Microbiol Biotechnol *36*, 19. https://doi.org/10.1007/s11274-020-2801-z.

6. Digel, L., Bonné, R., and Aiyer, K. (2024). Are all microbes electroactive? Cell Rep Phys Sci, 102200. https://doi.org/10.1016/j.xcrp.2024.102200.

7. Keogh, D., Lam, L.N., Doyle, L.E., Matysik, A., Pavagadhi, S., Umashankar, S., Low, P.M., Dale, J.L., Song, Y., Ng, S.P., et al. (2018). Extracellular electron transfer powers Enterococcus faecalis biofilm metabolism. mBio *9*. https://doi.org/10.1128/mBio.00626-17.

8. Pankratova, G., Leech, D., Gorton, L., and Hederstedt, L. (2018). Extracellular Electron Transfer by the Gram-Positive Bacterium Enterococcus faecalis. Biochemistry *57*, 4597–4603. https://doi.org/10.1021/acs.biochem.8b00600.

9. Light, S.H., Su, L., Rivera-Lugo, R., Cornejo, J.A., Louie, A., Iavarone, A.T., Ajo-Franklin, C.M., and Portnoy, D.A. (2018). A flavin-based extracellular electron transfer mechanism in diverse Gram-positive bacteria. Nature *562*, 140–157. https://doi.org/10.1038/s41586-018-0498-z.

10. Stevens, E.T., Van Beeck, W., Blackburn, B., Tejedor-Sanz, S., Rasmussen, A.R.M., Carter, M.E., Mevers, E., Ajo-Franklin, C.M., and Marco, M.L. (2023). Lactiplantibacillus plantarum uses ecologically relevant, exogenous quinones for extracellular electron transfer. mBio *14*. https://doi.org/10.1128/mbio.02234-23.

11. Basu, A., Manna, S., and Kumar Sil, A. (2023). A new electro-active bacterium, Paraclostridium sp. AKS46, converts waste efficiently into electricity in microbial fuel cell. Chemical Engineering Journal *475*. https://doi.org/10.1016/j.cej.2023.145626.

12. Conley, B.E., Weinstock, M.T., Bond, D.R., and Gralnick, J.A. (2020). A hybrid extracellular electron transfer pathway enhances the survival of vibrio natriegens. Appl Environ Microbiol *86*, 1–18. https://doi.org/10.1128/AEM.01253-20.

13. Nielsen, L.P., Risgaard-Petersen, N., Fossing, H., Christensen, P.B., and Sayama, M. (2010). Electric currents couple spatially separated biogeochemical processes in marine sediment. Nature *463*, 1071–1074. https://doi.org/10.1038/nature08790.

14. Pfeffer, C., Larsen, S., Song, J., Dong, M., Besenbacher, F., Meyer, R.L., Kjeldsen, K.U., Schreiber, L., Gorby, Y.A., El-Naggar, M.Y., et al. (2012). Filamentous bacteria transport electrons over centimetre distances. Nature *491*, 218–221. https://doi.org/10.1038/nature11586.

15. Bjerg, J.T., Boschker, H.T.S., Larsen, S., Berry, D., Schmid, M., Millo, D., Tataru, P., Meysman, F.J.R., Wagner, M., Nielsen, L.P., et al. (2018). Long-distance electron transport in individual, living cable bacteria. Proceedings of the National Academy of Sciences *115*, 5786–5791. https://doi.org/10.1073/pnas.1800367115.

16. Risgaard-Petersen, N., Kristiansen, M., Frederiksen, R.B., Dittmer, A.L., Bjerg, J.T., Trojan, D., Schreiber, L., Damgaard, L.R., Schramm, A., and Nielsen, L.P. (2015). Cable bacteria in freshwater sediments. Appl Environ Microbiol *81*, 6003–6011. https://doi.org/10.1128/AEM.01064-15.

17. Muyzer, G., Yildirim, E., Van Dongen, U., Kühl, M., and Thar, R. (2005). Identification of "Candidatus Thioturbo danicus," a microaerophilic bacterium that builds conspicuous veils on sulfidic sediments. Appl Environ Microbiol *71*, 8929–8933. https://doi.org/10.1128/AEM.71.12.8929-8933.2005.

18. Thar, R., and Kühl, M. (2002). Conspicuous veils formed by vibrioid bacteria on sulfidic marine sediment. Appl Environ Microbiol *68*, 6310–6320. https://doi.org/10.1128/AEM.68.12.6310-6320.2002.

19. Bjerg, J.J., Lustermans, J.J.M., Marshall, I.P.G., Mueller, A.J., Brokjær, S., Thorup, C.A., Tataru, P., Schmid, M., Wagner, M., Nielsen, L.P., et al. (2023). Cable bacteria with electric connection to oxygen attract flocks of diverse bacteria. Nat Commun *14*. https://doi.org/10.1038/s41467-023-37272-8.

20. Lustermans, J.J.M., Sereika, M., Burdorf, L.D.W., and Albertsen, M. (2024). Extracellular electron transfer genes expressed by candidate flocking bacteria in cable bacteria sediment.

21. Mandakovic, D., Cintolesi, Á., Maldonado, J., Mendoza, S.N., Aïte, M., Gaete, A., Saitua, F., Allende, M., Cambiazo, V., Siegel, A., et al. (2020). Genome-scale metabolic models of Microbacterium species isolated from a high altitude desert environment. Sci Rep *10*. https://doi.org/10.1038/s41598-020-62130-8.

22. Gneiding, K., Frodl, R., and Funke, G. (2008). Identities of Microbacterium spp. Encountered in Human Clinical Specimens. J Clin Microbiol *46*, 3646–3652. https://doi.org/10.1128/JCM.01202-08.

23. Nedelkova, M., Merroun, M.L., Rossberg, A., Hennig, C., and Selenska-Pobell, S. (2007). Microbacterium isolates from the vicinity of a radioactive waste depository and their interactions with uranium. FEMS Microbiol Ecol *59*, 694–705. https://doi.org/10.1111/j.1574-6941.2006.00261.x.

24. An, P., Yang, C., Li, W., Zhao, D., and Xiang, H. (2024). The Isolation and Characterization of a Novel Psychrotolerant Cellulolytic Bacterium, Microbacterium sp. QXD-8T. Microorganisms *12*. https://doi.org/10.3390/microorganisms12020303.

25. Spirina, E. V., Kuleshov, K. V., Yunusova, A.K., Vishnivetskaya, T.A., and Rivkina, E.M. (2019). Draft Genome Sequence of Microbacterium sp. Gd 4-13, Isolated from Gydanskiy Peninsula Permafrost Sediments of Marine Origin. Microbiol Resour Announc *8*. https://doi.org/10.1128/mra.00889-19.

26. Kageyama, A., Takahashi, Y., Matsuo, Y., Adachi, K., Kasai, H., Shizuri, Y., and Omura, S. (2007). Microbacterium flavum sp. nov. and Microbacterium lacus sp. nov., isolated from marine environments. Actinomycetologica *21*, 53–58. https://doi.org/10.3209/saj.saj210201.

27. Takeuchi, M., and Hatano, K. Union of the genera Microbacterium Orla-Jensen and Aureobacterium Collins et a/. in a redefined genus Microbacterium.

28. Plum-Jensen, L.E., Schramm, A., and Marshall, I.P.G. (2024). First single-strain enrichments of Electrothrix cable bacteria, description of E. aestuarii sp. nov. and E. rattekaaiensis sp. nov., and proposal of a cable bacteria taxonomy following the rules of the SeqCode. Syst Appl Microbiol *47*, 126487. https://doi.org/10.1016/j.syapm.2024.126487.

29. Lustermans, J.J.M., Bjerg, J.J., Schramm, A., and Marshall, I.P.G. (2021). Phyllobacterium calauticae sp. nov. isolated from a microaerophilic veil transversed by cable bacteria in freshwater sediment. Antonie Van Leeuwenhoek *114*, 1877–1887. https://doi.org/10.1007/s10482-021-01647-y.

30. O'Toole, G.A. (2010). Microtiter dish Biofilm formation assay. Journal of Visualized Experiments. https://doi.org/10.3791/2437.

31. Aiyer, K.S., and Vijayakumar, B.S. (2019). An improvised microtiter dish biofilm assay for non-invasive biofilm detection on microbial fuel cell anodes and studying biofilm growth conditions. Brazilian Journal of Microbiology *50*, 769–775. https://doi.org/10.1007/s42770-019-00091-5.

32. Schindelin, J., Arganda-Carreras, I., Frise, E., Kaynig, V., Longair, M., Pietzsch, T., Preibisch, S., Rueden, C., Saalfeld, S., Schmid, B., et al. (2012). Fiji: An open-source platform for biological-image analysis. Preprint, https://doi.org/10.1038/nmeth.2019 https://doi.org/10.1038/nmeth.2019.

33. Bolger, A.M., Lohse, M., and Usadel, B. (2014). Trimmomatic: A flexible trimmer for Illumina sequence data. Bioinformatics *30*, 2114–2120. https://doi.org/10.1093/bioinformatics/btu170.

34. Bankevich, A., Nurk, S., Antipov, D., Gurevich, A.A., Dvorkin, M., Kulikov, A.S., Lesin, V.M., Nikolenko, S.I., Pham, S., Prjibelski, A.D., et al. (2012). SPAdes: A new genome assembly algorithm and its applications to single-cell sequencing. Journal of Computational Biology *19*, 455–477. https://doi.org/10.1089/cmb.2012.0021.

35. Mikheenko, A., Prjibelski, A., Saveliev, V., Antipov, D., and Gurevich, A. (2018). Versatile genome assembly evaluation with QUAST-LG. In Bioinformatics (Oxford University Press), pp. i142–i150. https://doi.org/10.1093/bioinformatics/bty266.

36. Aronesty, E. (2013). Comparison of Sequencing Utility Programs.

37. Chklovski, A., Parks, D.H., Woodcroft, B.J., and Tyson, G.W. (2023). CheckM2: a rapid, scalable and accurate tool for assessing microbial genome quality using machine learning. Nat Methods *20*, 1203–1212. https://doi.org/10.1038/s41592-023-01940-w.

38. Seemann, T. (2014). Prokka: Rapid prokaryotic genome annotation. Bioinformatics *30*, 2068–2069. https://doi.org/10.1093/bioinformatics/btu153.

39. Li, W., and Godzik, A. (2006). Cd-hit: A fast program for clustering and comparing large sets of protein or nucleotide sequences. Bioinformatics *22*, 1658–1659. https://doi.org/10.1093/bioinformatics/btl158.

40. Fu, L., Niu, B., Zhu, Z., Wu, S., and Li, W. (2012). CD-HIT: Accelerated for clustering the next-generation sequencing data. Bioinformatics *28*, 3150–3152. https://doi.org/10.1093/bioinformatics/bts565.

41. Kanehisa, M., and Goto, S. (2000). KEGG: Kyoto Encyclopedia of Genes and Genomes.

42. Kanehisa, M., Sato, Y., and Morishima, K. (2016). BlastKOALA and GhostKOALA: KEGG tools for functional characterization of genome and metagenome sequences. J Mol Biol *428*, 726–731.

43. Camacho, C., Coulouris, G., Avagyan, V., Ma, N., Papadopoulos, J., Bealer, K., and Madden, T.L. (2009). BLAST+: architecture and applications BMC Bioinformatics 10: 421 doi: 10.1186.

44. Chaumeil, P.A., Mussig, A.J., Hugenholtz, P., and Parks, D.H. (2020). GTDB-Tk: A toolkit to classify genomes with the genome taxonomy database. Bioinformatics *36*, 1925–1927. https://doi.org/10.1093/bioinformatics/btz848.

45. Jain, C., Rodriguez-R, L.M., Phillippy, A.M., Konstantinidis, K.T., and Aluru, S. (2018). High throughput ANI analysis of 90K prokaryotic genomes reveals clear species boundaries. Nat Commun *9*. https://doi.org/10.1038/s41467-018-07641-9.

46. Abuyen, K., and El-Naggar, M.Y. (2023). Soluble Iron Enhances Extracellular Electron Uptake by Shewanella oneidensis MR-1. ChemElectroChem *10*. https://doi.org/10.1002/celc.202200965.

47. Roy, J.N., Garcia, K.E., Luckarift, H.R., Falase, A., Cornejo, J., Babanova, S., Schuler, A.J., Johnson, G.R., and Atanassov, P.B. (2013). Applied Electrode Potential Leads to Shewanella oneidensis MR-1 Biofilms Engaged in Direct Electron Transfer . J Electrochem Soc *160*, H866–H871. https://doi.org/10.1149/2.001401jes.

48. Carmona-Martinez, A.A., Harnisch, F., Fitzgerald, L.A., Biffinger, J.C., Ringeisen, B.R., and Schröder, U. (2011). Cyclic voltammetric analysis of the electron transfer of Shewanella oneidensis MR-1 and nanofilament and cytochrome knock-out mutants. Bioelectrochemistry *81*, 74–80. https://doi.org/10.1016/j.bioelechem.2011.02.006.

49. Zhao, J., Li, F., Cao, Y., Zhang, X., Chen, T., Song, H., and Wang, Z. (2021). Microbial extracellular electron transfer and strategies for engineering electroactive microorganisms. Preprint at Elsevier Inc., https://doi.org/10.1016/j.biotechadv.2020.107682 https://doi.org/10.1016/j.biotechadv.2020.107682.

50. Sturm, G., Richter, K., Doetsch, A., Heide, H., Louro, R.O., and Gescher, J. (2015). A dynamic periplasmic electron transfer network enables respiratory flexibility beyond a thermodynamic regulatory regime. ISME J *9*, 1802–1811. https://doi.org/10.1038/ismej.2014.264.

51. Rivera-Lugo, R., Huang, S., Lee, F., Méheust, R., Iavarone, A.T., Sidebottom, A.M., Oldfield, E., Portnoy, D.A., and Light, S.H. (2023). Distinct Energy-Coupling Factor Transporter Subunits Enable Flavin Acquisition and Extracytosolic Trafficking for Extracellular Electron Transfer in Listeria monocytogenes. mBio *14*. https://doi.org/10.1128/mbio.03085-22.

52. Engel, M., Bayer, H., Holtmann, D., Tippkötter, N., and Ulber, R. (2019). Flavin secretion of Clostridium acetobutylicum in a bioelectrochemical system - Is an iron limitation involved? Bioelectrochemistry *129*, 242–250. https://doi.org/10.1016/j.bioelechem.2019.05.014.

53. Lustermans, J.J.M., Bjerg, J.J., Burdorf, L.D.W., Nielsen, L.P., Schramm, A., and Marshall, I.P.G. (2023). Persistent flocks of diverse motile bacteria in long-term incubations of electron-conducting cable bacteria, Candidatus Electronema aureum. Front Microbiol *14*. https://doi.org/10.3389/fmicb.2023.1008293.

54. Franco, A., Elbahnasy, M., and Rosenbaum, M.A. (2023). Screening of natural phenazine producers for electroactivity in bioelectrochemical systems. Microb Biotechnol *16*, 579–594. https://doi.org/10.1111/1751-7915.14199.

55. Otero, F.J., Chan, C.H., and Bond, D.R. (2018). Identification of different putative outer membrane electron conduits necessary for Fe(III) citrate, Fe(III) oxide, Mn(IV) oxide, or electrode reduction by geobacter sulfurreducens. J Bacteriol *200*. https://doi.org/10.1128/JB.00347-18.

56. Jahan, M.I., Juengwiwattanakitti, P., Izu, Y., Tobe, R., Imai, T., and Mihara, H. (2019). Selenite uptake by outer membrane porin ExtI and its involvement in the subcellular localization of rhodanese-like lipoprotein ExtH in Geobacter sulfurreducens. Biochem Biophys Res Commun *516*, 474–479. https://doi.org/10.1016/j.bbrc.2019.06.037.

571 57. Thorup, C., Petro, C., Bøggild, A., Ebsen, T.S., Brokjær, S., Nielsen, L.P., Schramm, A., and Bjerg,
572 J.J. (2021). How to grow your cable bacteria: Establishment of a stable single-strain culture in
573 sediment and proposal of Candidatus Electronema aureum GS. Syst Appl Microbiol *44*.
574 https://doi.org/10.1016/j.syapm.2021.126236.

575